Energy science master thesis

Searching for optical gain in colloidal silicon nanocrystals

Author:
Bart van Dam

Carried out at:
Tom Gregorkiewicz Group (WZI–UvA)

Supervisors:
Dr. Kateřina Dohnalová (UvA)
Prof. dr. Tom Gregorkiewicz (UvA)
Dr. Wilfried G.J.H.M. van Sark (UU)

Second reader:
Boudewijn Elsinga (MSc,UU)

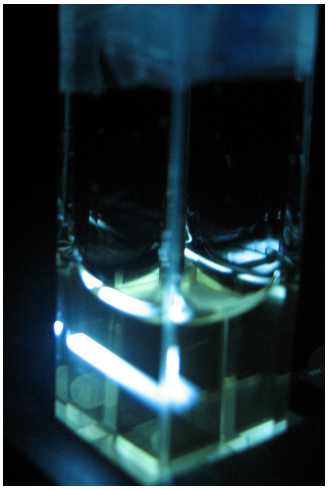

July 18, 2013

Abstract

Optical gain in silicon nanocrystals (NCs) faces two major loss factors that prevent lasing activity: depopulation by fast Auger recombination and a low effective NC concentration due to the finite size distribution. The improved radiative rates in carbon passivated silicon nanocrystals, might constitute the solution to the detrimental effect of depletion of the inverted population by Auger interactions. In this research optical spectroscopy is combined with the variable stripe length (VSL) and shifting excitation spot (SES) method to study optical gain in colloidal samples of methyl and butyl capped silicon nanocrystals, made by wet–chemical synthesis. Deviation of VSL from SES indicates the presence of amplified stimulated emission in the samples. The optical gain, however, is low in comparison to length of the excited stripe, which is expected to be inherent to the finite particle size distribution and total NC concentration in the system.

Contents

1 Introduction

1.1 Interconnections bottleneck

Silicon (Si) is abundant, non–toxic and has electronic properties that led to undisputed dominance in the microelectronics industry. However, the decreasing chip size imposes limits on the speed, space and power consumption of the metal interconnects that are used for information transfer [1]. To overcome this so called interconnections bottleneck, there is large interest for the integration of optical elements such as lasers into microelectronic devices. Efficient direct band gap emitters exist, e.g. InP and GaAs, but integrating these into the silicon-based chip is expensive and the formed hetero–structures affect the material quality.

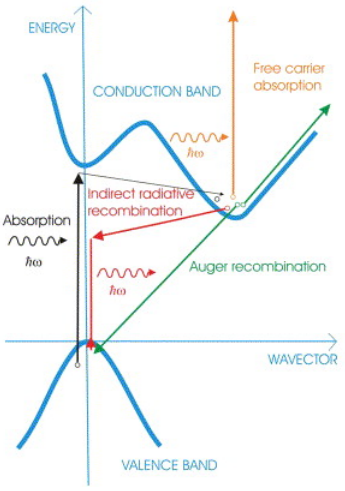

Figure 1: Schematic illustration of indirect band gap nature of silicon: phonon-assisted absorption and spontaneous emission, Auger recombination and free carrier absorption [1].

The monolithic solution, bulk silicon, seemingly comprises the ideal candidate. Unfortunately silicon is for this purpose unsuitable, due to poor radiative properties arising from the indirect band gap (figure 1). Associated radiative transitions require a phonon to ensure conservation of momentum and are suppressed as a result of the low probability of this three particle process. As a result radiative decay is overshadowed by non–radiative electron–hole recombination at defect sites and due to Auger recombination. Moreover, a notoriously known paper by Dumke [2] in 1962 depreciated bulk silicon as possible active medium for laser applications. His theoretical calculations showed that due to the low radiative rates, absorption by free carriers would kill the amplified stimulated emission, which is the principle lasers operate on[1].

1.2 Optical gain in silicon nanocrystals

In 1990 hope for a silicon based laser was revived, when emission in the visible range was observed in nano–scale silicon crystals [3, 4]. The potential barrier at the interface of a nanocrystal (NC) and the surrounding dielectric, e.g. SiO_2 confines and localizes the electronic states within the nanocrystal (quantum confinement). Consequently, as a result of Heisenberg's uncertainty principle, the condition of conservation of momentum 'relaxes': wave functions of the electrons in the conduction band and holes in the valance band overlap and

[1] Additionally, a cavity is required to maintain lasing activity, a pumping mechanism to excite carriers and to achieve population inversion, e.g. by carrier injection or optical pumping and a select resonant wavelength range.

the probability of radiative decay increases; No-phonon radiative recombination becomes weakly allowed. Additionally, the optical band gap increases with respect to that of bulk silicon ($E_g = 1.12$ eV) with decreasing NC size as a result of the confining surface potential. Hence, controlling the NC size facilitates tuning of the photoluminescence (PL), shifting towards the visible range for sizes <5 nm [5]. These enhanced optical properties boosted the idea of using a system of silicon nanocrystals to achieve optical gain and lasing.

Up to now, however, a theoretical basis of optical gain in silicon NC ensembles has not fully been established [5]. Moreover, the study of low–gain materials is not straightforward. Experimental techniques have been developed to distinguish low gain values among various losses, but interpretation of these results is difficult. Nonetheless different reports, e.g. [6, 7, 8, 9], provide experimental confirmation of positive optical gain in dense ensembles of oxidized Si NCs. Still however, radiative rates are slow compared to fast nonradiative processes; Especially Auger recombination depletes the population inversion and hence strongly competes with optical gain [6]. Moreover, fabrication processes yield a broad size distribution of Si NCs, so that only a fraction of NCs is in resonance and can contribute to stimulated emission of certain frequency [5]. Scattering due to inhomogeneity and aggregation in the sample further contributes to losses. As a result, active lasing cannot be maintained and therefore, still, the first laser with silicon as active medium remains to be built.

1.3 Research goal

Recently, carbon-passivated colloidal silicon quantum dots (diamater 2.2 ± 0.5 nm), made by wet chemical synthesis were shown to have more efficient band–edge absorption and enhanced, tunable emission in the visible range, corresponding to direct band gap–like transitions in the core of the Si NCs [10]. These improved optical properties make carbon–passivated Si QDs highly interesting for applications in different fields, among other things, photovoltaics, bio–imaging and light–emitting diodes (LEDs). Likewise, the increased radiative rates (factor 100-1000 compared to oxidized Si NCs) are expected to significantly improve the conditions for optical gain, as radiative transitions are able to compete with non-radiative recombination processes (Auger). Moreover, the C-passivation prevents the nanocrystals from aggregating, hence reducing scattering losses. In this research optical gain in carbon-passivated Si NCs is investigated.

2 Theory

2.1 Silicon nanocrystals

Bulk silicon is an indirect band gap semiconductor: the top of the valence band and the bottom of the conduction band are misaligned in k–space. Consequently, radiative transitions require a phonon to satisfy conservation of momentum.

This three–particle process is of low probability compared to non–radiative transitions, such as Auger recombination, free carrier absorption (FCA) or defect trapping. Figure 1 illustrates the indirect band gap and the main non–radiative channels.

By localization of carriers within the potential that arises between the Si NC and the surrounding dielectric, silicon's optical properties are strongly affected. With the diameter of a NC approaching the exciton Bohr radius (4.9 nm for silicon), Coulombic interactions between carriers become increasingly important. For sizes < 5 nm excitons can be modeled as a 'particle in a box' resulting in discrete energy levels and opening of the band gap (see figure 2). Furthermore, it follows from Heisenberg uncertainty principle that the momentum conservation condition relaxes and non-phonon radiative transitions become weakly allowed. This results in an increase in radiative rates compared to bulk silicon.

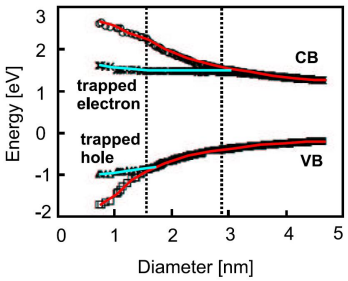

Figure 2: The optical band gap of silicon as a function size, with trap states originating from Si-O bonds. Adapted from [11].

2.1.1 Surface passivation

Aside from size, the optical properties of nanocrystals strongly depend on composition, surroundings and surface geometry, which can be achieved by using different manufacturing methods, e.g. ion implantation, chemical vapor deposition, colloidal synthesis, sputtering etc. [5]. Enhancementof optical quality of Si NCs revolves around increasing the probability of radiative recombination, while reducing non-radiative events. The former is achieved by quantum confinement; The latter involves, among others, reducing efficient non–radiative trapping defects that exist at the NC surface as a result of dangling bonds. This is achieved by careful passivation of the surface, for which hydrogen and oxygen are frequently used. However, H– and O–passivated Si NCs both have relatively long radiative decay times ($\sim \mu s$) and moreover, H–passivated NCs are unstable [8]. Besides, as a result of fixed defect states originating from oxigen–related defects at the surface, the PL of O-passivated Si NCs is not tunable within the visible range of the spectrum [11]. This is visualized in figure 2, where fixed defect–realted trapping statesat the surface of the NC are revealed when the optical band gap opens up. In case of carbon ternmination the situation is very different. Due to the electro–negativity of carbon atoms at the surface, electrons are drawn to the surface leading to further carrier localization. Hence, the carbon passivation induces additional changes to the e–h wavefunctions, resulting in direct like band gap radiative rates [10]. Figure 3 illustrates the effect of different surface capping atoms on Si NCs.

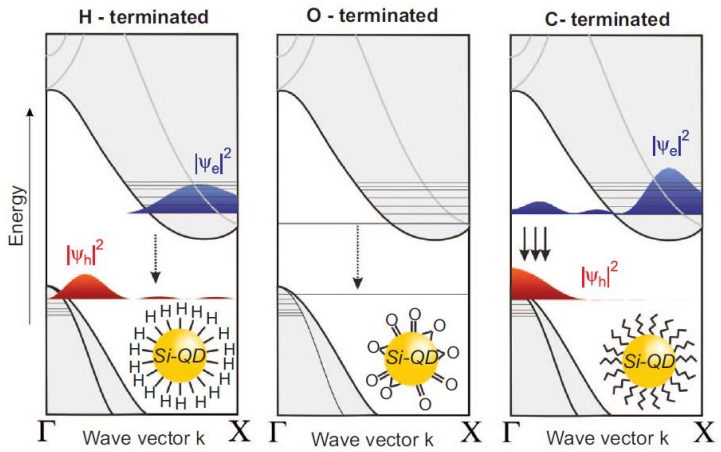

Figure 3: Schematic illustration of the band gap and associated radiative transitions in H–, O– and C–passivated silicon nanocrystals. Broadening of the wave functions indicates the effect of quantum confinement. H–passivation yields weak quantum confinement and quasi-direct band gap radiative transitions. Oxygen–passivation induces surface defects that dominate radiative decay. Direct band gap like transitions are found in C-passivated Si NCs. [10]

2.2 Optical properties of silicon nanocrystals

2.2.1 Photoluminescence

Carriers which are excited by photon absorption can relax to the valence band via spontaneous emission[2], resulting in PL. Carbon passivated Si NCs were shown to exhibit bright PL in the visible range, inherent to direct like band gap transitions in the Si NC core. The broad PL spectrum is a result of inhomogeneous broadening of the system comprising a size distribution of Si NCs (diameter of 2.2 ± 0.5 nm). The band–to–band absorption characteristics allow the PL to be tuned over the range of $\sim$ 460–560 nm, by controlling the excitation energy and hence selecting NCs with $E_g < E$ [10].

2.2.2 Non–radiative channels

As mentioned briefly, different non–radiative channels contribute to depletion of the excited carrier population, i.e. non–radiative recombination at defects sites, Auger recombination and FCA. Surface defects can be reduced by careful surface architecture, passivating the dangling bonds that exist at the surface. Additionally, since $\alpha_{FC} \propto \lambda^2$, free carrier absorption in nanocrystals is significantly reduced compared to bulk material due to the opening of the optical band

[2]Alternatively, carriers might recombine via stimulated emission. This will be extensively discussed in section 2.3.1

gap [12]. The rate of non-radiative Auger interactions however, is enhanced in nanocrystals, as it strongly depends on the volume in which excited carriers are contained. Auger recombination, however, is limited by the condition of multiple excitons present in a NC, $N \geq 2$. For $N \geq 2$, the Auger lifetime is assumed to decrease as $\tau_{Auger} \sim R^3$ with NC size as empirically established by [13] and is in the order of ns [14].

2.2.3 Photoluminescence lifetime

The time evolution of the PL intensity is governed by an exponential decay with a characteristic lifetime τ_{PL}, where the PL decay rate $(1/\tau_{PL})$ is given by the sum of the radiative and non–radiative decay rates: $\frac{1}{\tau_{PL}} = \frac{1}{\tau_{rad}} + \frac{1}{\tau_{nrad}}$. Due to quantum confinement, NC size directly affects the radiative rate and therefore in Si NC ensembles, the PL decay time comprises a distribution of recombination rates. Hence in systems where size is strongly correlated to the decay rate, decay is described by the stretched exponential function [15]:

$$I_{PL} = I_0 e^{-(t/\tau)^{-\beta}}. \tag{1}$$

Here $0 < \beta < 1$ is the dispersion factor. $\beta = 1$ signifies single exponential behavior, whereas $\beta < 1$ indicates a distribution of decay times. In systems with direct band gap lifetime, there is negligible size–dependence and stretched exponential behavior of the PL lifetimes is not present.

2.2.4 Quantum yield

PL external quantum yield (QY) is commonly used to characterize the optical efficiency of a material. It is defined as the ratio of the number of emitted photons by a system to the number of absorbed photons:

$$\text{QY} = \frac{\#\text{ emitted photons}}{\#\text{ absorbed photons}}. \tag{2}$$

Non–radiative channels provide alternative recombination routes for excited carriers. The QY therefore indicates the weight of radiative–decay in the PL decay. High QY does not necessarily imply high radiative rates, as it might also result from suppression of non-radiative channels; Even slow PL will be visible in absence of non-radiative channels that deplete the excited carrier concentration.

2.3 Light amplification through stimulated emission

2.3.1 Stimulated emission

Lasers are based on the principle of light amplification through stimulated emission: i.e. coupling of the electromagnetic field of a resonant photon to the electric field of an excited e–h pair and subsequent recombination under emission of a 'clone' of the original photon. Stimulated emission is the inverse absorption process, in which a photon couples to a carrier in the ground state and excites it to a higher energy state. The probability of absorption and stimulated emission differs only in the population densities of carriers in the contributing state, which are the ground and excited states respectively. Within a cavity, for light traveling along the cavity axis, the contribution of spontaneous (isotropic) emission can be neglected and the absorption coefficient, as a result of spontaneous emission, stimulated emission and absorption, in bulk semiconductors reads [12]:

$$\alpha_0(\nu) = (N_1 - N_2) \cdot \sigma_{op}(\nu) = (N_1 - N_2)\frac{c^2}{8\pi\nu^2 t_{sp}}\gamma(\nu - \nu_0) \quad [cm^{-1}]. \tag{3}$$

Here, σ_{op} is the absorption cross–section (optical cross-section), N_1 and N_2 denote the population densities of electrons in the ground state and excited state, ν is the frequency of the light, t_{sp} the spontaneous emission lifetime, $\gamma(\nu - \nu_0)$ is the distribution of the spectral line around ν_0 and c the speed of light in vacuum. In thermodynamic equilibrium when the majority of the electrons is in the ground state, $N_1 \gg N_2 \Leftrightarrow N_1 \approx N$, absorption dominates and light is attenuated as it travels through the medium, with the evolution of the intensity described by the Lambert-Beer law:

$$I_\nu(z) = I_\nu(0)e^{-\alpha_0(\nu)z}. \tag{4}$$

In order to achieve the non-equilibrium state where amplified stimulated emission (ASE) can prevail, population inversion is to be achieved, $N_2 > N_1$. Upon population inversion, $\alpha_0(\nu) < 0$ and following equation 4 light is amplified. Negative absorption is called optical gain, with the gain coefficient $g(\nu)$ given by the negative absorption coefficient as in equation 3,

$$g(\nu) = -|\alpha_0(\nu)| = (N_2 - N_1) \cdot \sigma_{op}(\nu). \tag{5}$$

Since the number of electrons in the system is constant $N_1 + N_2 = N$, the maximum value of $g(\nu)$ is achieved for $N_2 = N$. The absorption of the material therefore puts an upper limit to the optical gain. This is an important consideration as it shows that not only efficient emission, i.e. fast radiative decay rate $1/t_{sp}$, but also efficient absorption is required for optical gain, which is proportional to the optical cross-section.

2.3.2 Population inversion

It can be shown [16] that in a system consisting of only two levels, population inversion cannot be achieved. As the number of excited carriers increases under intense pumping, the absorption saturates and the feedback by stimulated emission increases. Ultimately, an equilibrium state is reached where absorption and stimulated emission rates balance out: $N_1 = N_2$. Additional energy levels are required to maintain population inversion, with specific conditions for the lifetime of these levels. Figure 4 shows a three- and four-level system in which population inversion can be achieved. Both consist of an additional superior energy state $E_3 > E_2$ with short decay time compared to the lower level. Carriers pumped to this level, quickly relax into E_2 and are consequently trapped for some time thus increasing N_2, as a result of the relatively long radiative lifetime τ_{21}. A three-level system, however, requires strong pumping in order to empty E_1 and thus further increase the popualtion inversion $N_2 - N_1$. A four-level system has a additional sub-band gap level that allows quick emptying of the lower energy state of the transition of interest ($E_2 \rightarrow E_1$). To achieve a significant difference in lifetimes, three- and four-level systems usually require defects states [3] to trap carriers for some time, e.g. such as seen in oxygen–terminated quantum dots [11, 6].

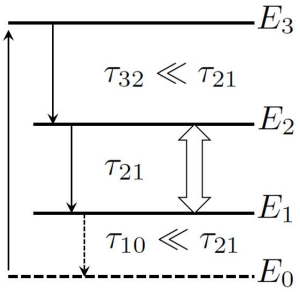

Figure 4: Conditions for the lifetimes of a three-(solid lines) and four-level (solid and dashed lines) system required to achieve population inversion between levels E_2 and E_1.

2.3.3 Net optical gain in nanocrystals

The gain discussed in section 2.3.1 is commonly referred to as the material optical gain. To achieve net gain, there are additional loss mechanisms that have to be overcome, which have an attenuating effect on the ASE. As discussed in the introduction, dominant losses in nanocrystals comprise absorption by free carriers, absorption by defects, scattering and Auger recombination. Loss factors are collectively captured by $K(\nu)$; The net gain thus reads, $G(\nu) = g(\nu) - K(\nu)$ and similarly in case of absorption $\alpha_{tot}(\nu) = \alpha_0(\nu) + K(\nu)$. In section 2.2 the reduction of FCA in Si NCS compared to bulk silicon was already discussed. Furthermore, scattering losses can be reduced by surface passivation, preventing the nanocrystals from aggregating[4] and moreover reducing dangling bonds that exist at the surface.

The rate of non-radiative Auger recombination however, is enhanced in NCs. When multiple excitons are localized within a NC, as a result of strong pumping for inverted population, Auger recombination becomes more efficient. Due to the indirect band gap, silicon nanocrystals ensembles are primarily affected

[3] I.e. levels E_2 and E_1.
[4] This applies to colloidal systems.

by non-radiative Auger recombination. Therefore, an additional condition for positive optical gain is that the stimulated emission lifetime can compete with the lifetime of Auger recombination [12]:

$$\tau_{stim} = \frac{n}{cg} = \frac{n}{n_0 \rho \sigma_{op} c} < \tau_{Auger}. \tag{6}$$

Here n is the refractive index and $g = n_0 \rho \sigma_{op}$ is the analogy to equation 5 for nanocrystals, with $n_0 \cdot \rho$ the number density of nanocrysals where population inversion has been achieved ($0 \leq \rho \leq 1$). Equation 6 gives important information on improving the conditions for optical gain in silicon quantum dot ensembles:

- High optical cross-section σ_{op}: efficient absorption and short radiative lifetimes. Moreover, suppression of non-radiative effects.
- Population inversion $\rho \to 1$.
- High nanocrystal concentration n_0

Somewhat related to the last condition, the nanocrystal size distribution plays a major role: large size distribution (i) reduces the effective concentration of silicon nanocrystals and (ii) enhances losses due to scattering and (re-)absorption. Condition (i) arises from the resonant character of stimulated emission. In NCs, the optical band gap and corresponding radiative transitions are related to NC size. Hence, only a fraction of nanocrystals contributes to stimulated emission of specific frequency and following equation 6 the rate of stimulated emission is reduced. Besides, larger NCs with $E_g < E_{photon}$ can reabsorb the stimulated emission or contribute to scattering in the sample.

2.4 Determination of optical gain

2.4.1 Variable stripe length

The most frequently applied technique for the detection of optical gain is the Variable Stripe Length (VSL) method proposed by Shaklee et al. in 1971 [17]. Emission from a sample is detected perpendicular to the incident laser beam, which excites a stretched-rectangular shaped part of the sample. In essence this is a pump and probe experiment, where the excitation beam is used as pump and where spontaneous emission from the sample functions as the probing beam. A moving slit is used to vary the length of this stripe; The setup is schematically depicted in figure 5.a. Without ASE, the spontaneous emission signal is attenuated and the detected intensity I_{ASE} as function of stripe length is obtained by integrating $I_{sp} \cdot e^{-\alpha_{tot} x}$ over the stripe length l. Contrary in case of light amplification, optical gain manifests itself as the exponential increase of the detected ASE intensity as function of stripe length:

$$I_{ASE} = I_{sp}(\nu) \cdot \int_0^l e^{G(\nu)x} dx = \frac{I_{sp}(\nu)}{G(\nu)} (e^{G(\nu)l} - 1). \tag{7}$$

The spectrum of the gain coefficient can be calculated from the ratio of the ASE intensity of stripe length l and $2l$. It can be show that [12]:

$$G(\lambda) = \frac{1}{l} \ln \left(\frac{I_{ASE}(2l, \lambda)}{I_{ASE}(l, \lambda)} \right). \tag{8}$$

Equation 7 is funded on two assumptions: (i) constant coupling efficiency (given by a coupling function $\beta(x) = \text{cst}$) of emission to detector, i.e. no dependence along the stripe on detector light collecting efficiency and an (ii) one-dimensional, homogeneous excitation stripe to ensure constant pumping power (P(x)) along the stripe and to maintain the initial intensity of the probing beam independent of distance, $I_{sp}(x) = I_{sp}$ [18]. These conditions are experimentally not easily satisfied, as will be discussed in the next section.

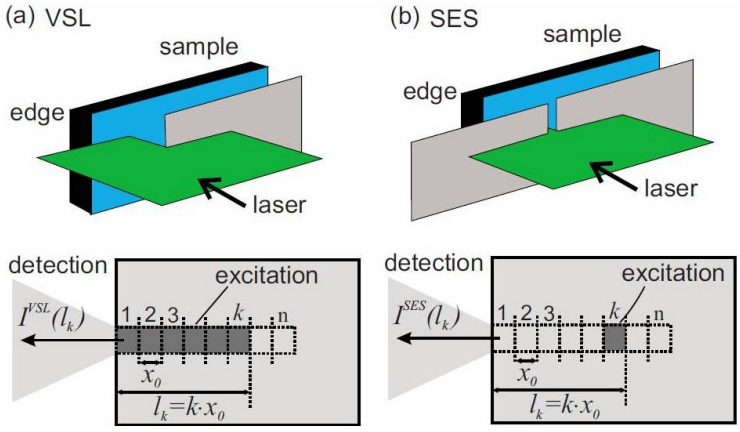

Figure 5: Left: schematic representation of VSL excitation beam illuminating a striped-part of the sample. Emission is detected perpendicular to the excitation beam. By moving the adjustable slit (gray), stripe length can be varied along the x–axis. Right: by addition of a second slit, the stripe is reduced to a spot (SES). The excitation spot is moved along the VSL stripe to produce a reference without ASE [19].

Apart from these conditions, it is assumed that population inversion is maintained. In case of strong light amplification, however, the ASE quickly depletes the population density of excited carriers for longer stripe length, resulting in the saturation of gain. In case of gain saturation, population inversion is governed by [16]:

$$(N_2 - N_1)_{sat} = \frac{N_2 - N_1}{1 + \Phi/\Phi_{sat}}. \tag{9}$$

Here Φ equals the photon flux, and Φ_{sat} the saturation photon flux. From equation 5 it follows that the gain coefficient saturates and reduces by the same factor.

2.4.2 Experimental artifacts

It was shown, that interpretation of the results obtained by VSL for low-gain materials is not straightforward. First of all, the technique is sensitive only for sufficiently large gain, $Gl \gg 1$: when $Gl \ll 1$, $e^{GL} \approx 1 + Gl$ and equation 7 reduces to $I_{ASE} \approx I_{PL}l$, independent of G. Additionally, the experimental setup in practice never satisfies the assumptions where the VSL method is based on and $P_{exc}(x)$, $\beta(x)$ and $I_{sp}(x)$ are usually x–dependent. The arising artifacts distort the VSL measurements and might even result in incorrect observation of optical gain [20]. The major effects that influence the coupling efficieny of emission to the detection system are are discussed below.

- *Waveguiding*: the high fluence of the excitation beam can induce changes in refractive index, creating a waveguiding layer in the sample. This waveguide enhances especially the detected intensity of spontaneous emission, which is collimated towards the detection system. Additionally, the angle at which the signal leaves the sample is larger for emission closer to the sample edge. Light exiting with an angle that is larger than the numerical aperture (NA) of detection is lost and therefore can result in the apparent increase in I_{ASE} for longer stripe [20]. Waveguiding is expected to be minimal in colloids, due to NC diffusion in the liquid environment and due to enhanced heat dissipation compared to solid state samples.

- *Confocal effect*: the detection system is aligned to collect light from the edge of the excited stripe. A set of two lenses with large numerical aperture, focused on the sample edge ($l_f = 0$ mm), is used to increase the collection efficiency. In this configuration coupling efficiency of emission originating beyond the depth of focus, $xl >$ DOF, given by the approximate relation DOF $\approx \lambda/\text{NA}$ [18] is reduced as it is imaged in front of the detector. Artificial increase can occur when the focal plane lies significantly deep inside the sample. In this case, collection efficiency for stripe length increasing towards the position of the focal plane $0 < l < l_f$ increases, which can lead to a false observation of optical gain.

- *Beam homogeneity*: a laser with rectangular beam profile is most suited for VSL experiments, whereas for Gaussian beam profiles, only part of the beam can be used. Furthermore the beam profile and intensity can be altered by Fresnel diffraction from the edge of the adjustable slit. As a result (i) the beam profile becomes non-rectangular and (ii) the power of the excitation beam (P) becomes stripe length dependent. Moreover the probe signal becomes a function of distance $I_{sp}(x)$. Increase in pump intenstiy by diffraction occurs at small stripes and can therefore result in an apparent increase in the ASE intensity.

2.4.3 Shifting excitation spot

In order to monitor (and correct for) artifacts, the shifting excitation spot method, introduced by [20], can be used alongside VSL measurements. SES

comprises of a second slit so that the stripe is reduced to a spot, which is subsequently moved along the VSL stripe (see figure 5.b). The spot is to be sufficiently small so that no light amplification takes place within the spot: $\Delta x \ll \frac{1}{G}$; Usually the spot width is taken equal to the increment of the VSL stripe. Since for SES there is no excitation in between the spot and the sample edge towards the detector, population in this part is not inverted. Consequently only spontaneous emission originating from the excited spot contributes, which is attenuated as a result of absorption and other losses in the unexcited region. For the ideal case, i.e. constant detection efficiency and homogeneous beam, SES intensity is given by:

$$I_{SES}(\nu, x) = I_{sp}(\nu) \cdot e^{-\alpha_{tot} x}. \tag{10}$$

By summing the contributions of all SES measurements along the VSL stripe a reference is created without stimulated emission. For infinitely small steps, this yields:

$$I_{intSES} = I_{sp}(\nu) \cdot \int_0^l e^{-\alpha_{tot}(\nu) x} dx = I_{sp}(\nu) \cdot \frac{1 - e^{\alpha_{tot}(\nu) l}}{\alpha_{tot}(\nu)}. \tag{11}$$

In a non-ideal case, the coupling efficiency $\beta(x)$ and inhomogeneity in probe signal $I_{sp}(\nu, x)$ should be accounted for. Moreover, G and α_{tot} are x–dependent due to difference in pumping power along the stripe. Infinitesmal increase in intSES and VSL can be expressed as[5] [21]:

$$dI_{intSES}(\nu, x) = \beta(x) \left[\alpha_{tot}(\nu, x) \cdot I_{intSES}(\nu, x) + I_{sp}(\nu, x)\right] dx \tag{12}$$

$$dI_{ASE}(\nu, x) = \beta(x) \left[G(\nu, x) \cdot I_{ASE}(\nu, x) + I_{sp}(\nu, x)\right] dx. \tag{13}$$

It is in practice, however difficult to extract $I_{sp}(\nu, x)$ and $\beta(x)$ from SES measurements. Nonetheless, while used alongside VSL, SES can help in distinguishing artefacts from the experimental results. If the intSES displays exponential increase in intensity, the VSL–determined gain is at least partially artificial. Contrary, if the VSL signal is significantly larger than that of intSES for larger stripe, VSL–intSES$>$ 0, this indicates the presence of non-linear phenomena such as stimulated emission.

2.4.4 Power dependence and spectral narrowing

Another fingerprint of the presence of optical gain is the abrupt change from linear to super–linear dependence of the ASE intensity on the excitation power [17]. This on a log–log scale is inherent to an increase of the slope. For G approximately proportional to pumping power, $G \propto (n_0 \rho) \sim P$, Gl will increase with excitation intensity. Under low pumping, when $Gl \ll 1$, $e^{GL} \approx 1 + Gl$, equation 7 reduces to $I_{ASE} \approx I_{PL} l$. When $Gl > 1$, stimulated emission overcomes losses, leading to a super–linear dependence on pumping power: $I_{ASE} \propto P^{\gamma}$, with $\gamma > 1$. On the other hand, sub–linear dependence indicates the dominance by

[5] Note the explicit x–dependence of involved parameters.

either gain saturation or non-radiative processes, e.g. Auger recombination in case of multiple excitons per NC or photo–chemical deterioration in the sample. The exact slope corresponding to each phenomenon depends on specific sample properties. Nonetheless, the presence of a clear super–linear slope in the power dependence is strong evidence of stimulated emission, whereas (sub)linear dependence indicates absence of stimulated emission.

Furthermore, stimulated emission is accompanied by narrowing of the spectrum compared to that of spontaneous emission. In case of ASE, the contribution of resonant photon energies, corresponding to transitions between levels of inverted population, is enhanced. Hence for stronger ASE, the spectrum narrows around this transition's frequency. The ratio of the FWHM of the ASE and SpE spectrum, assuming a Gaussian distribution, is given by the Linford equation [22]:

$$\frac{\Delta\nu_{ASE}}{\Delta\nu_0} = \sqrt{\frac{G-1}{G\,\ln G}} \tag{14}$$

The contribution of stimulated emission frequency is more pronounced in a system consisting of particles with identical transition frequencies, e.g. atoms or molecules, where the spectrum results from homogenous broadening. The contribution of a single frequency will increase with ASE for the entire system and the spectrum narrows. In a system where the spectral shape is controlled by inhomogeneous broadening, overal emission results from a distribution of transition frequencies. In Si NC ensembles, this is due to different particles sizes. Only part of the NCs contribute to ASE of specific frequency and with ASE, spectral narrowing might occur for each of these sub–systems. However, the overall narrowing is smoothed out by the frequency (size) distribution in the entire system.

3 Methodology

3.1 Sample preparation

Samples were purchased from The Chemical Research Solution (TCRS), prepared following a wet chemical synthesis method [23], which was adapted from Kauzlarich et al. [24]. First magnesium silicide is oxidized with bromine, forming bromine-terminated Si NCs. These were subsequently passivated, yielding methyl (CH_3) an butyl (C_4H_9) capped Si NCs, with a typical size of 2.2 ± 0.5 nm. For analysis, the nanocrystals are dispersed in UV–grade ethanol to obtain colloidal samples; The concentration of these samples has not been defined.

3.2 Excitation spectrum and absorption

Excitation spectrum was measured with a SPEX Fluorolog3–22 over an excitation range of 320-600 nm. Transmission, T through a cuvette (1 cm) was obtained by a spectrophotometer (Lambda 950, Perkin Elmer), from which absorption coefficients were calculated: $\alpha = \ln(1/T)$ [cm^{-1}]. Absorption measure-

ments were carried out with the sample both outside and inside an integrating sphere to correct for scattering losses.

3.3 Photoluminescence decay time

PL decay time was measured under 355 nm excitation, supplied by the frequency–doubled signal of a tunable Ti:Sapphire laser (Chameleon Ultra, Coherent). Repetition rate was reduced from 80 MHz to 8 MHz by a pulse picker (PulseSelect, APE). PL was detected using a monochromator (M20, Carl Zeiss) coupled to a photomultiplier tube (R3809U-50, Hamamatsu). The instrumental response time of the system was determined from scattered laser light on a dilute colloidal silica sample and yields ∼23 ps (FWHM).

3.4 Quantum yield

PL external quantum yield was determined by measuring emission and transmission of both the sample and a reference (ethanol) sample, following the concept developed by [25]. A Xenon lamp (Hamamatsu) was used as excitation source, coupled with an optical fiber to an integrating sphere (Newport). The samples were placed inside the integrating sphere to average out the directionality of emission and to account for reflection and scattering. The sphere is fiber-coupled to the detection system, composed of a spectrometer (M266, Solar Laser Systems) coupled to a charge-coupled device (CCD, Hamamatsu).The detection system's spectral response, $SR(\lambda)$, was determined using a tungsten halogen lamp (Oriel, 250-2400 nm) and a deuterium lamp (Oriel, 200-400 nm). Pixel to wavelength conversion was calibrated using the spectral lines of a mercury lamp (Oriel)[6]. The detected intensity, $i(\lambda)$ was corrected for the spectral sensitivity of the setup and converted to an energy scale, correcting for the fact that the used spectrometer is linear in wavelength: $I(eV) = i(\lambda) \cdot SR(\lambda) \cdot \lambda^2$ [12]. The grating of the spectrometer allows a spectral window of detection of $\sim$ 400 nm and was configured to capture both excitation light and PL in the same window. Conversion to energy scale is required to enable extraction of the PL spectrum and excitation spectrum by fitting it with a Gaussian distribution, as direct integration is not possible due to the overlap between the excitation spectrum and the broad PL spectrum of the Si NCs. For the fitting procedure of the PL, both excitation peak and its 2nd order harmonics were excluded from the detection signal. QY is then determined as:

$$QY = \frac{\sum\limits_{emission} \left(I_{sample}(E_{em}) - I_{ref}(E_{em})\right)/E_{em}}{\sum\limits_{excitation} \left(I_{sample}(E_{exc}) - I_{ref}(E_{exc})\right)/E_{exc}}. \tag{15}$$

Here *sample* and *ref* denote the NC sample and reference sample respectively. The sum in the numerator runs over the emission band and the sum in the denominator runs over the excitation band. Since correction for the spectral

[6] See e.g. [26, 27] for a detailed description of the calibration procedure.

response yields $I(\text{eV})$ in units of energy, division by the photon energy, E_{em} and E_{exc} respectively, therefore gives the number of photons.

3.5 Optical gain

The stripe-shaped excitation beam for the VSL setup is supplied by the third harmonic (355 nm) of a solid state Nd:YAG laser, with 7 ns pulses and a repetition rate of 100 Hz. For power dependence measurements, the beam is attenuated by a Glan-Thompson polarizer prism. Provided that the beam is fully polarized, this allows to tune the excitation power between approximately 0 and 100%. Using a cylindrical lens (focal length of 10 cm), the Gaussian beam is then focused in vertical direction, after which the width in horizontal (x) direction is controlled by a movable slit/shield. A set of convergent lenses with a magnification ratio of 2:1 is placed between the slit and sample to reduce diffraction effects on the edge of the slit/shield. With a beam profile meter (Spiricon) the homogeneous part of the stripe is then determined, as well as the minimum SES spot width that has acceptable diffraction effects. For the corresponding settings of the motor controlling the adjustable slit, the VSL and SES measurements are then carried out. The detection system consist of a set of lenses with NA$\sim$ 0.22, focused on the sample edge. The lasing signal of a cuvette filled with Rhodamine 6G, a high gain medium, solved in ethanol was used to align the detection system with the axis of stimulated emission in the sample. Moreover, Rhodamine 6G was used to validate the ability of the setup to detect optical gain.

4 Results: radiative characterization

4.1 Photoluminescence and absorption

Absorption spectra $\alpha_{tot}(\lambda)$ were measured with the samples outside and inside of an integrating sphere. An integrating sphere will account for scattering losses, i.e. $\alpha_{tot} = \alpha_0$, whereas without an integrating sphere scattering losses will be seen by the detection system as absorption $\alpha_{tot} = \alpha_0 + K$. Both measurements yield similar results, implying that scattering in the samples is minimal: $K \approx 0$. The absorption spectra are shown in figure 6.

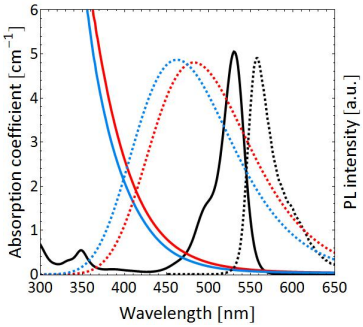

Figure 6: Linear absorption coefficient, $\alpha_0(\lambda)$, (solid lines, left axis) and PL (dashed lines, right axis) for Rhodamine 6G (black) and methyl (red) and butyl (blue) capped Si NCs.

The excitation spectra of the Si NCs are shown in figure 7. Furthermore, the excitation spectrum at maximum PL intensity ($\sim$ 518 nm), is shown in figure 8, peaking at 410 nm for both samples. The PL spectrum corresponding to excitation of 355 nm, which is

used for VSL experiments, is shown in figure 6 (dashed lines). The respective PL peaks are situated around 480 and 460 nm for methyl and butyl capped Si NCs respectively and at 556 nm for R6G. It follows from figure 8 that PL intensity under 355 nm excitation is an order of magnitude lower than at 410 nm excitation. Experimentally, VSL setup for the silicon samples can thus be improved upon by exciting with 410 nm, provided similar pumping power can be achieved[7]. R6G is a molecule with characteristic narrow–band absorption around 530 nm, which also corresponds to the excitation maximum.

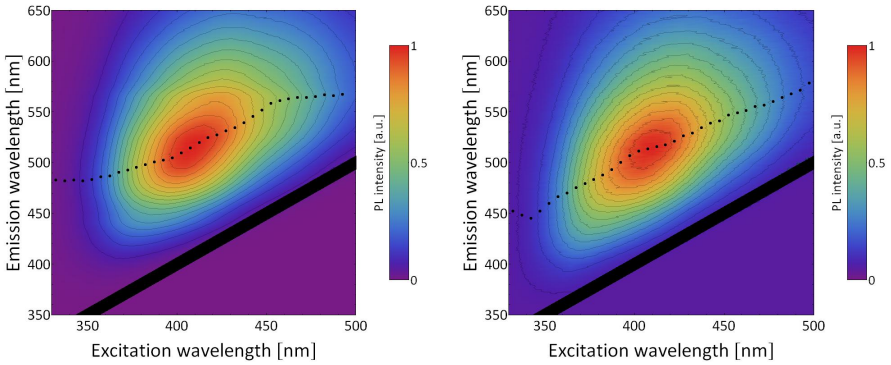

Figure 7: Excitation spectrum of methyl capped (left) and butyl capped (right) Si NCs. The black line indicates the scattered excitation light, the black dots indicate the PL peak position for every excitation wavelength.

For the NC ensembles, a large Stokes shift is observed, meaning that the samples are optically transparent to their emission, i.e. there is a mismatch between absorption and emission preventing emission to be instantly re–absorbed. Moreover, comparison of the tunability of the emission wavelength of methyl and butyl capped Si NCs is illustrated in figure 8 (values taken from figure 7). It follows that butyl capping allows for a broader tuning of emission. This is possibly due to additional modification of the e–h wavefunctions due to longer carbon–chains at the the surface. Direct transitions are characterized by excitonic absorption peaks and allow better size selection.

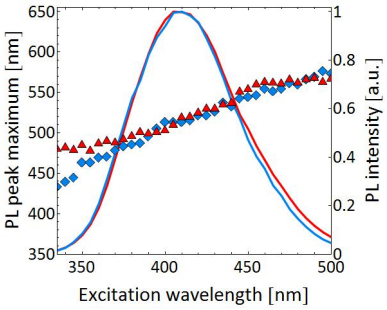

Figure 8: Excitation spectrum at emission wavelength of 518 nm (solid lines, right axis) and wavelength corresponding to PL peak as function of excitation wavelength (symbols, left axis) for methyl (red) and butyl (blue) capped Si NCs.

[7]In our experimental setup this is not the case. 355 nm excitation is used as it yields the highest output power.

4.2 Photoluminescence lifetimes

Following [28] the PL decay was fitted with a triple exponential decay function:

$$I_\lambda(t) = \sum_{i=1}^{3} A_i \cdot e^{-t/\tau_i}, \tag{16}$$

where the first exponential was configured to fit the first few picoseconds of the decay, corresponding to the instrumental response time of the setup (∼23 ps), which probably results from stray light. The results for the two remaining components are plotted in figure 9. PL decay times are in good agreement with those found for butyl terminated quantum dots in [29, 10, 28], corresponding to intrinsic direct-like radiative transitions in carbon terminated NCs. The results are given in figure 9. Both types of passivation yield similar PL lifetimes. The process corresponding to the fast component (0.5–0.8 ns) is most likely a trapping state.

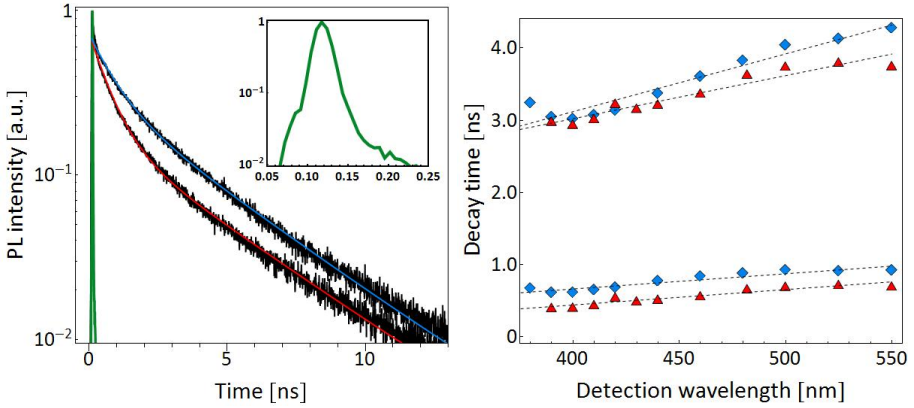

Figure 9: Left: peak PL evolution in time (black curves) and triple exponential fit for methyl capped (red, 482 nm) and butyl capped (blue, 460 nm) Si NCs. Green curve around 0 ns represents the system's signal response time (see inset). Right: PL decay times for different detection wavelengths, dashed lines are a guide to the eye (red: methyl capped Si NCs, blue: butyl capped Si NCs).

4.3 Quantum yield

QY was determined using equation 15, the results are shown in figure 10. The measured QY of butyl capped Si NCs is in good agreement with the QY reported for butyl capped Si NCs in [28]. The QY of methyl–capped Si NCs, is 1-4% lower. Apart from surface passivation, the Si NCs are fabricated in the same way and moreover, decay times were shown to be approximately equal (see figure 9). Assuming only a difference in surface passivation, this implies that butyl capping results in more suppression of non–radiative effects than methyl capping. Possibly, the larger butyl molecules are more efficient in preventing oxygen from diffusing in the NC or the butyl passivation process itself is more efficient than the corresponding process for methyl.

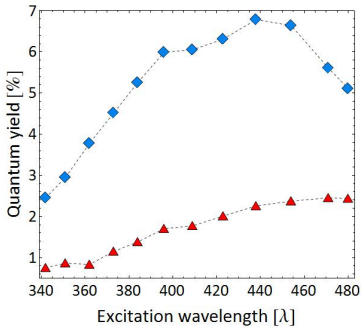

Figure 10: PL quantum yield versus excitation wavelength for methyl (red) and butyl (blue) passivated Si NCs.

5 Results: optical gain

5.1 Beam profile and SES

Two sets of measurements were performed. An indication of the profile of the excitation beam for both measurements is shown in figure 11. Both measurements were performed under slightly different conditions, resulting in a shorter maximum stripe length in the second set[8]. The experimental quality of the setup is monitored by the SES method, of which the results plotted figures 12 and 13. Ideally, the focal plane of the detection system is at the sample edge and the SES signal as function of distance is governed by equation 10.

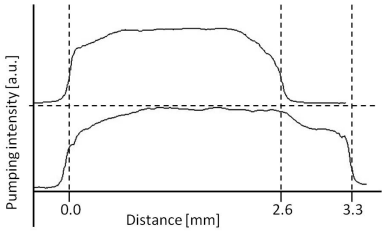

Figure 11: Beam profiles, shifted along the y-axis, as measured under low pumping power for the first (bottom) and second (top) set of measurements. Width (FWHM) of corresponding SES signals is 0.25 and 0.15 mm respectively.

5.1.1 First set of measurements

The measurement, however, deviates from this ideal case, as the SES signal displays an initial rise towards some critical length $0 < l < l_c$, beyond which the decay sets in. l_c is defined by the maximum of the SES intensity and comprises 0.9 and 0.6 mm for the both silicon samples and Rhodamine 6G respectively. As discussed in section 2.4.2, the shift of the critical length away from the sample

[8] E.g. the influence of laser maintenance in between both measurements on the excitation beam.

edge ($x = 0$) is due to the combination of a gradual increase of the pumping power with stripe length and stripe-dependent coupling efficiency to the detection system [9]. The former is caused by the beam profile of the excitation laser which is not ideal for VSL measurements and possibly by diffraction effects on the movable slit edges. The confocal effect mainly contributes to the light coupling efficiency; The effect of waveguiding as a result of pumping induced changes in the refractive index is expected to be minimal in colloids, as discussed in section 2.4.2.

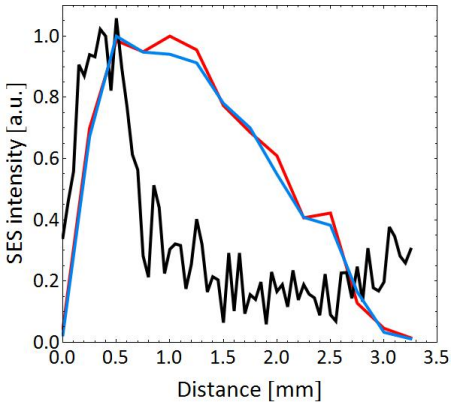

Figure 12: Measured evolution of SES signal at 477 nm as function of distance from the sample edge; Methyl capped (red) and butyl capped (blue) Si NCs, with SES–stepsize of 250 μm; Black line represents Rhodamine 6G at 550 nm, with SES–stepsize of 100 μm.

The consequences of $l_c > 0$ are: (i) at least part of the initial rise in $I_{ASE}(0 < l < l_c)$ is due to experimental artifacts and (ii) the effective stripe length is reduced by $\sim l_c$. Both consequences are problematic when gain is small and longer stripes are required to reveal the dependence of equation 7.

Since experimental conditions are equal, the difference between the critical length for R6G and for the silicon samples arises from difference in the attenuation coefficient α_{tot}. For stronger attenuation $I_{SES}(l_c)$ shifts towards smaller l. In the first set of measurements this however could not be verified; α_{tot} could not be determined due to strong deviation from $I_{SES}(\nu, x) = I_{sp}(\nu) \cdot e^{-\alpha_{tot} x}$ caused by coupling effects and beam inhomogeneity.

5.1.2 Second set of measurements

The results for the second set of measurements[10] are shown in figure 13. Methyl and butyl capped Si NCs both display $l_c \approx 1.2$ mm. The exponential decrease beyond the critical length, governed by equation 10 is conserved and α_{tot} can be extracted, yielding $\alpha_{tot,Si}(477 \text{ nm}) \approx 13 \text{ cm}^{-1}$. For Rhodamine 6G in this set of measurements the SES setup was slightly altered, by moving the focus of the detection system away from the sample. By doing so the critical length is reduced to $l_c \approx 0.5$ mm (black curve, for similar value of $\alpha_{tot,R}(477 \text{ nm}) \approx 13 \text{ cm}^{-1}$). This illustrates the large influence of the confocal effect.

[9] Note that the maximum value of I_{SES} follows from the convolution of these effects with attenuation of stimulated emission in the sample.

[10] Note that R6G (black and gray lines) was measured under slightly different conditions.

Moreover, the effect of attenuation on the critical length is demonstrated by comparison of the SES signal of Rhodamine 6G at 477 and 550 nm, yielding $\alpha_{tot,R}(550\text{ nm}) \approx 22\text{ cm}^{-1}$. For almost doubling of α_{tot} the critical length is reduced by 0.2 mm. The silicon samples have somewhat constant $\alpha_{tot}(\lambda)$ and do no show this shift. It should be noted that the loss coefficients that are found are

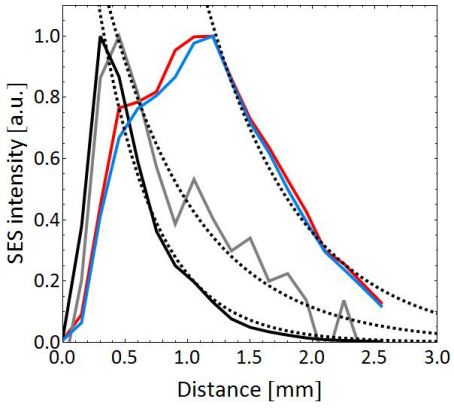

Figure 13: Measured evolution of SES signal at 477 nm as function of distance from the sample edge. Rhodamine 6G (gray), methyl capped (red) and butyl capped (blue) Si NCs, with SES–step size of 150 μm; Dotted lines are fits by equation 10 yielding $\alpha_{tot} \approx 13\text{ cm}^{-1}$. Additionally, Rhodamine 6G is also shown for 550 nm (black line), displaying higher total losses $\alpha_{tot} = 22\text{ cm}^{-1}$

more than an order of magnitude larger than the linear absorption coefficient of R6G and more than two orders of magnitude larger for both silicon samples (see section 4.1), yielding[11] $\alpha_{0,Si}(477\text{ nm}) \approx 0.04\text{ cm}^{-1}$, $\alpha_{0,R}(477\text{ nm}) \approx 0.6\text{ cm}^{-1}$ and $\alpha_{0,R}(477\text{ nm}) \approx 1.12\text{ cm}^{-1}$. This implies that either (i) loss mechanisms strongly attenuate the signal, $K > \alpha_0$ or that (ii) either excitation power or SpE detection efficiency decreases towards the end of the stripe, causing an additional apparent attenuating effect. The latter might result in irregularities in SES decay, such as seen for the first set of measurements. The effect of high K is likely to conserve the exponential character of the decay of I_{SES}. However, it was already concluded from absorption measurements (section 4.1) that additional losses (scattering) are minimal in the samples and therefore $\alpha_{tot} \approx \alpha_0$. This further indicates the strong presence of artifacts (ii).

5.2 VSL and intSES

Both VSL and SES spectra were corrected for the spectral sensitivity of the detection system. Subsequently, the intSES signal was obtained by summing the contributions of the detected SES spectra along the stripe $\text{intSES}(l) = \sum_0^l \text{SES(x)}$. IntSES was normalized to match the VSL signal for short stripe lengths ($l \sim 500$ μm), by linear regression. In this regime spontaneous emission dominates and VSL and intSES are equal in theory; However experimental discrepancy between both may occur when there is overlap or gap between subsequent SES spots along the stripe. After this normalization step, deviation of VSL from intSES for larger stripe indicates the presence of nonlinear phenomena such as light amplification through stimulated emission.

[11] Values for methyl capped Si NCs are taken here, absorption for butyl is slightly lower.

5.2.1 Rhodamine 6G

The results for the first set of measurements for Rhodamine 6G are shown in figure 14. It indicates the difference between the detected VSL and integrated SES signals and provides an indication where to look for optical gain. The maximum is found slightly red–shifted from the PL peak, at $\sim$ 572 nm.

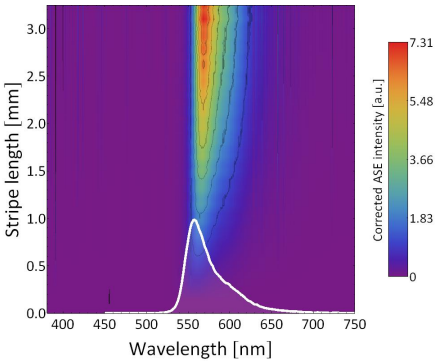

Figure 14: Corrected ASE intensity (=VSL–intSES) for Rhodamine 6G under 0.03 mJ, 355 nm excitation. White line indicates the PL spectrum.

VSL and intSES signals are shown in more detail in figure 15. At the observed maximum in figure 14 at 572 nm, exponential increase is seen in the VSL signal. The exponential rise in the intSES signal, however, confirms the findings of section 5.1 that at least part of the initial rise of ASE is artificial. Nonetheless, a rough indication of the gain coefficient can be obtained by using equation 7, neglecting the contribution of the artificial rise. This approximation yields a gain coefficient: $G \sim 6$ cm^{-1}. The theoretical upper limit for the value of the gain coefficient is set by the linear absorption coefficient, which is at 572 nm more than two orders of magnitude smaller ($\alpha_0(572\text{ nm}) = 0.03$ cm^{-1}, see figure 6). Therefore the obtained net gain coefficient must be due to multiple passages through the stripe, with the cavity provided by the reflective cuvette walls. In this experiment single–passage is assumed and therefore the real gain coefficient is overestimated by at least a factor equal to the number of reflections. The right panel in figure 15 furthermore demonstrates occurrence of gain saturation, for shorter wavelengths (560 nm and $l > 1.2$ mm), where the exponential increase in ASE flattens out.

5.2.2 Silicon nanocrystals

Results for the silicon samples are shown in figures 16. It follows that maximum gain can be expected around the respective PL peaks for both types of Si NCs. For these wavelengths VSL and intSES signals are in detail plotted in figure 17. Poor normalization can easily result in a positive difference VSL–intSES and therefore care should be taken when interpreting these results.

Figure 17 shows a linear rise in VSL, which indicates $Gl < 1$. Moreover intSES measurements reveal that the initial part of this rise is due to an experimental artifact, as discussed in section 5.1. If any gain is present in this system, the experimental maximal stripe length is thus insufficient to reveal it. Equation 7 can therefore not be used to extract the gain coefficient and likewise equation 8 will not hold for its spectral dependence. Nevertheless, deviation between the ASE signal and the SES signal for larger stripes indicates the presence of

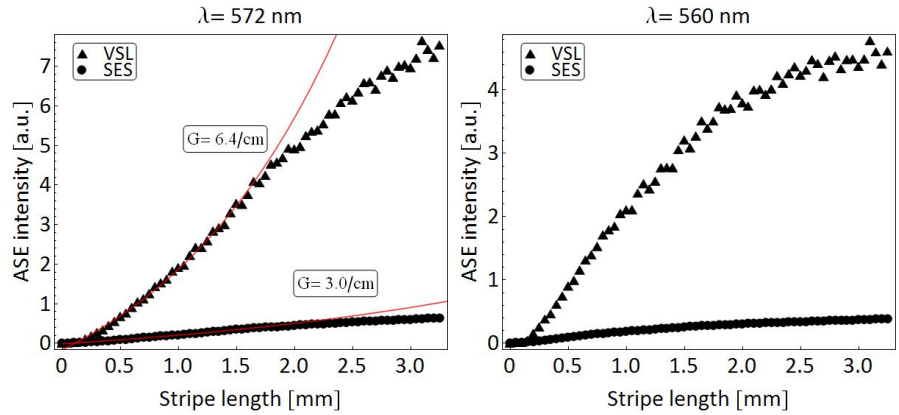

Figure 15: Detailed plot of VSL (triangles) and intSES (dots) signal at 572 nm (left) and 560 nm (right) under 355 nm excitation and 0.03 mJ pumping. Fitting equation 7 yields $G(572) \approx 6$ cm^{-1}. intSES shows also exponential increase, yielding an artificial gain of 3 cm^{-1}. Right panel shows gain saturation.

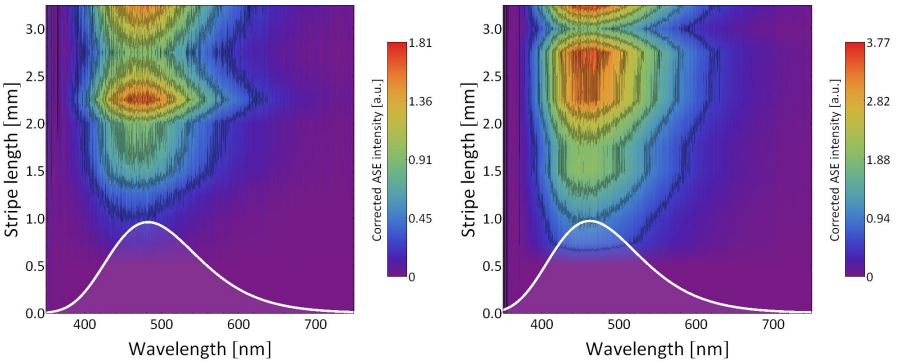

Figure 16: Corrected ASE intensity (=VSL–intSES) for methyl (left) and butyl (right) capped Si NCs under 0.1 mJ, 355 nm excitation. White line indicates the PL spectrum.

stimulated emission. Furthermore the absolute positive difference between VSL and intSES increases with pumping intensity, which could be an indication of increased gain coefficient as a result of increase of the fraction of NCs where population inversion is achieved. Interesting to note is that while the absolute difference between VSL and intSES changes, the shape of the curves displayed in figure 17 remain similar throughout the spectral range of the experiment (not shown here). This might point towards a range of resonant frequencies, corresponding to the finite size distribution of the silicon NCs. As a result, the effective number density of NCs contributing to stimulated emission of certain frequency ν is low and hence $G(\nu) < \frac{1}{l}$.

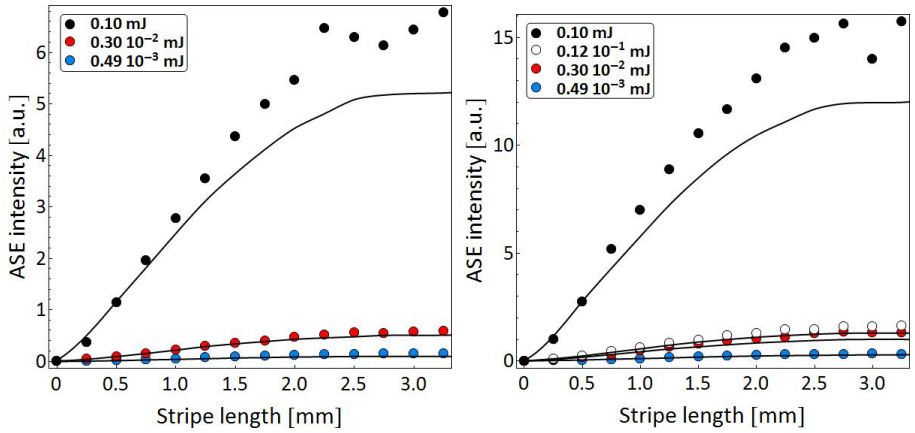

Figure 17: Detailed plot of VSL (symbols) and intSES (solid lines) signal at the wavelength of maximal difference between VSL and intSES (see figure 16). Methyl (left, 478 nm) and butyl (right, 460 nm) capped Si NCs under 355 nm excitation for different pumping intensities (see inset). For both silicon samples, the VSL shape is similar for different wavelengths; However, the absolute difference between VSL and intSES varies.

5.3 Power dependence

In order to link the observed difference between VSL and intSES in the silicon samples to stimulated emission, power dependence measurements were carried out. For a constant stripe length, 2.2 and 2.4 mm for the first and second set of measurements respectively, the excitation power was varied using a Glan-Thompson prism.

5.3.1 Rhodamine 6G

Threshold behavior that signifies the presence of light amplification is illustrated for Rhodamine 6G in figure 18. At 572 nm, I_{ASE} changes from $\sim P^1$ to $\sim P^{2.4}$, at a pumping threshold of 60 μJ. For reference, different wavelength are plotted which do not show this jump. Combined with the VSL and intSES data, this provides conclusive evidence of stimulated emission.

5.3.2 Silicon nanocrystals

In figure 19, the relation between I_{ASE} and pumping power is plotted for the Si NCs of both measurements[12]. The observed drop in intensity between the first (triangles) and second (dots) measurements is due to different experimental conditions, e.g. shorter CCD exposure time, difference in detection efficiency

[12]Note that only relative excitation power was determined for the first set of measurements, i.e. rotation angle of Glan-Thompson prism, θ. The maximum absolute power (P_0 was estimated by comparing the intSES intensity with that of the intSES intensity of the second set of measurements, from which other powers were calculated: $P = P_0(0.5 + 0.5\ \mathrm{Sin}(2\theta))$

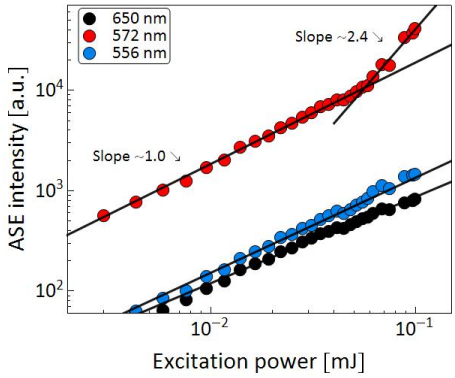

Figure 18: Dependence of ASE intensity on pumping power for R6G for three different wavelengths. At a pumping threshold of 60 μJ abrupt change in power dependence is observed $P^1 \rightarrow P^{2.4}$

etc. Originally, the second set of measurements (dots) was performed in order to study the apparent increase in slope around 0.1 mJ in the first set of measurements in more detail. However, the slope remains linear for the methyl capped Si NCs and drops to sub–linear ($I_{ASE} \sim P^{0.7}$) for butyl. The observation of linear power dependence in both sets of measurements provides strong evidence against net optical gain.

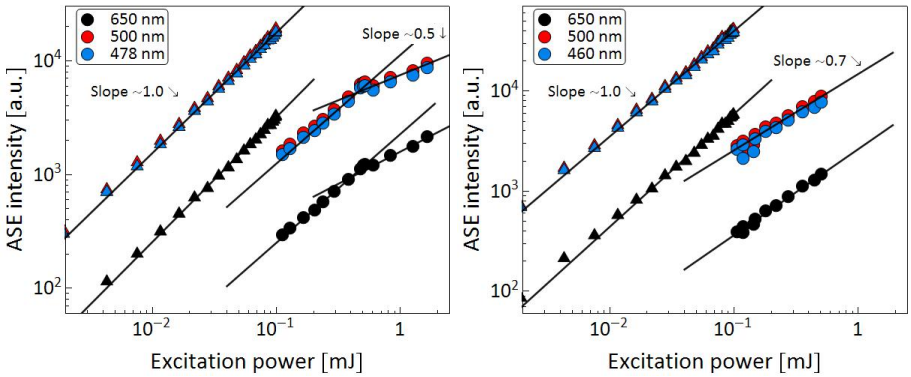

Figure 19: Dependence of ASE intensity on pumping power for methyl (left) and butyl (right) capped Si NCs for three different wavelengths. Black lines are linear fits and correspond to power of the dependence, i.e. given by the slope on log–log scale, associated to parts of the data set. Triangles and dots represent the first and second set of measurements respectively.

For powers above 0.06 mJ, the power dependence of methyl displays a decrease to $I_{ASE} \sim P^{0.5}$, suggesting Auger or even photo–chemical deterioration of the sample, $g < K$. To prevent damage, these high powers were not repeated for the butyl–capped Si NCs, as it already showed to be in sub–linear regime. It should be noted however that to prevent damage to the Glan-Thompson, the prism was removed for high excitation flux $P > 0.5$ mJ. Therefore, the excitation beam does not pass through the Glan-Thompson in the last few points of the

left panel in figure 19 (methyl), which introduces differences to the beam profile, for which the setup was not optimized. This beam profile was not determined due to the low damage threshold of the beam profile meter. Assuming, however, that both dependencies are inter–comparable, two explanations possible explanations can be suggested for the transition to sub–linear regime:

- Population inversion is not achieved in the system. There are no known defect levels in carbon passivated Si NCs and therefore a three–or four–level system might not be present. Upon increasing excitation power, multiple excitons can be present within a NC and Auger interactions are enhanced. Once $K > g$ as a result of Auger recombination, power dependence enters the sub–linear regime.

- Population inversion is achieved, however, owing to the finite size distribution, the effective fraction of NCs with inverted population contributing to resonant emission of frequency ν, $\rho \cdot n_0(\nu)$, is low. For increase in pumping power beyond the point where $\rho \cdot n_0$ is maximum, again Auger recombination is enhanced.

5.4 Spectral narrowing

To provide supporting evidence for the presence of optical gain, the spectrum of the ASE signal was compared to that of the spontaneous emission; The results are plotted in Figure 20. No spectral narrowing is observed for both silicon samples, i.e. equation 14 results in $\frac{\Delta\nu_{ASE}}{\Delta\nu_0} \sim 1$. This does not necessarily argue against optical gain in NC ensembles as studied here. Contribution of the individual NC spectra in an ensemble is averaged out by the size distribution [21].

For Rhodamine 6G, no spectral narrowing is observed at 0.03 mJ. Under 0.1 mJ excitation, however, spectral narrowing of 0.6 is observed. The excitation power is well above the ASE threshold and the narrowing here might be attributed to lasing, as multiple passages are already involved under 0.03 mJ excitation (see section 5.2). This argument is supported by observation of lasing in Rhodamine 6G by the naked eye.

Another observation of spectral change is observed in the shift of ASE spectrum towards higher wavelengths. This observation indicates re–absorption in the sample, which can be significant especially for longer stripes; Following the absorption coefficient in figure 6, shorter wavelengths are absorbed more strongly leading to the observed shift. For Rhodamine 6G, where a strong absorption peak 'hugs' the emission and where light passes the sample multiple times, this effect is more pronounced. In Si NC ensembles re–absorption can play an important role as it contributes to attenuation of the stimulated emission.

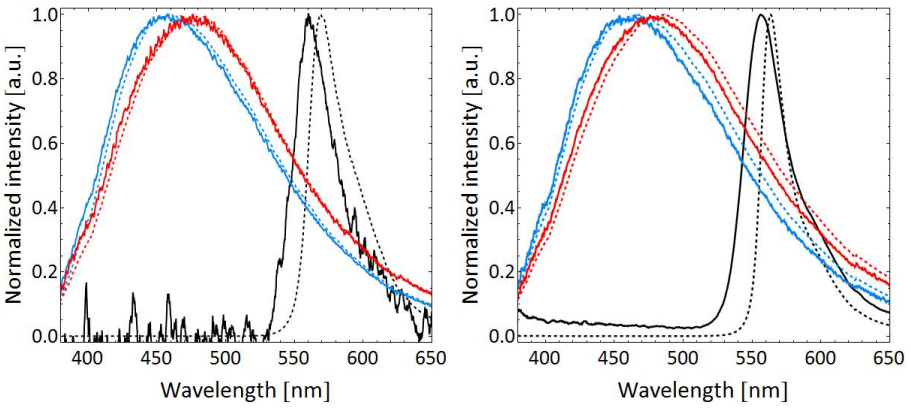

Figure 20: PL intensity (solid lines) and ASE at maximum stripe length (dashed lines) spectra for Rhodamine 6G (black) and methyl capped (red) and butyl capped (blue) Si NCs under 355 excitation. Panels correspond to the first (left) and second (right) set of measurements. Corresponding excitation intensities are left: 0.03 mJ (R6G) and 0.1 mJ (methyl and butyl capped); Right: 0.11 mJ (R6G), 0.48 mJ (methyl capped) and 0.15 mJ (butyl capped). Intensity of Rhodamine 6G below 520 nm is noise that is amplified in the normalization step.

5.5 Conclusions: optical gain in Si NCs

Despite improved optical properties and a positive difference between VSL and intSES intensity, conclusive evidence for optical gain was not found for studied carbon-passivated Si NCs. Contrary, (sub)linear dependence of ASE intensity on pumping power provides evidence for $Gl \ll 1$, or even $g < K$ under high pumping power. These findings can be attributed to the experimental setup or to limitations inherent to material properties:

- The experimental setup has serious limitations, which complicate interpretation of the results of low gain measurements: (i) coupling of emission to the detection is not constant and (ii) the excitation beam is inhomogeneous and allows only for a maximum stripe of ∼3 mm. Since the gain, if any, is expected to be low, the maximum stripe length might have been insufficient to reveal an exponential increase in the ASE intensity. Moreover, the critical stripe length, further reduces the effective path length of the amplifying medium, mainly due to the confocal effect and beam inhomogeneity.

- Apart from experimental limitations, it could be that population inversion is not achieved in this system. There are no known defect levels present in the material and therefore a three–or four–level system might not be present. Upon increasing excitation power to attempt to achieve a larger fraction of population inversion, Auger interactions are enhanced and corresponding losses, $K > g$. This might explain the sub–linear slope in power dependence upon high excitation fluence. Alternatively, population

inversion might be achieved, but due to the small effective number density of NCs with resonant frequencies, gain is small. Again Auger recombination is enhanced under stronger pumping. Re–absorption of stimulated emission by NCs without inverted population further reduces the stimulated emission. These consideration point out that size distribution plays an important role, due to the resonant character of stimulated emission [5].

6 Recommendations

To proceed from these findings several points of improvement can be suggested to optimize the conditions for optical gain and for detection of optical gain. Most importantly, the effective NC concentration should be maximized, by increasing the total NC concentration and decreasing the size polydispersity. The latter will be challenging due to the practical limits of existing fabrication methods. However, increasing concentration will directly improve the optical gain coefficient and hence the ability to compete with Auger recombination. The maximum gain value can then be estimated by measuring the absorption coefficient. This will give an indication of the length of the stripe, $l > 1/\alpha$ in VSL method that is required to reveal the optical gain (if present). The VSL setup can be improved, apart from of expensive optics to improve the beam homogeneity, by choosing an excitation wavelength corresponding to the peak of the excitation spectrum, provided that high pumping powers can be achieved. This will result in stronger probing signal and therefore stronger overall emission. Finally, careful alignment of the detection system is of great importance to reduce experimental limitations.

Acknowledgments

First of all, I would like to thank Tom for the opportunity to do this master project and for letting me be part of his group. I want to thank Katerina for the supervision, useful discussions, instructions and feedback. I appreciate that you could always find time for my questions, despite your busy schedule. Thirdly, I want to express my gratitude towards the group (TGG), which provides for a relax and inspirational working environment. I much appreciate the teamwork and cohesion in the group, also on a non–research related basis, e.g. the BBQs and the Futsal tournament. Some random shout–outs: the working out sessions (Rens), the struggles with deconvolution ("Thou shall not deconvolute", Elinore) and "You–Did" (Chung).

Moreover, I want to thank Michiel and Tatu from the Chemistry department for the decay dynamics measurements (I hope to maintain further collaboration in the future), Leon Webbers for using his automated VSL script and Wilfried and Boudewijn for the external support.

References

[1] L Pavesi. Silicon-based light sources for silicon integrated circuits. *Advances in Optical Technologies*, 2008, 2008.

[2] WP Dumke. Interband transitions and maser action. *Physical Review*, 127(5):1559–1563, 1962.

[3] LT Canham. Silicon quantum wire array fabrication by electrochemical and chemical dissolution of wafers. *Applied physics letters*, 57:1046–1048, 1990.

[4] H Takagi, Ogawa H, Y Yamazaki, A Ishizaki, and T Nakagiri. Quantum size effects on photoluminescence in ultrafine si particles. *Applied physics letters*, 57:2379–2380, 1990.

[5] VA Belyakov, VA Burdov, R Lockwood, and A Meldrum. Silicon nanocrystals: fundamental theory and implications for stimulated emission. *Advances in Optical Technologies*, 1:1–32, 2008.

[6] L Dal Negro, M Cazzanelli, N Daldosso, Z Gaburro, L Pavesi, F Priolo, D Pacifici, G Franzo, and F Iacona. Stimulated emission in plasma-enhanced chemical vapour deposited silicon nanocrystals. *Physica E: Low-dimensional Systems and Nanostructures*, 16(3):297–308, 2003.

[7] K Dohnalová, I Pelant, K Køusová, P Gilliot, M Gallart, O Crégut, JL Rehspringer, B Hönerlage, T Ostatnickỳ, and S Bakardjeva. Closely packed luminescent silicon nanocrystals in a distributed-feedback laser cavity. *New Journal of Physics*, 10(6):063014, 2008.

[8] K Dohnalová, K Židek, L Ondič, K Køusová, O Cibulka, and I Pelant. Optical gain at the f-band of oxidized silicon nanocrystals. *J. Phys. D: Appl. Phys.*, 42:1–5, 2009.

[9] K Luterová, K Dohnalová, V Švrček, Ivan Pelant, J-P Likforman, Olivier Crégut, Pierre Gilliot, and Bernd Hönerlage. Optical gain in porous silicon grains embedded in sol-gel derived sio matrix under femtosecond excitation. *Applied physics letters*, 84:3280, 2004.

[10] K Dohnalová, AN Poddubny, AA Prokofiev, WDAM de Boer, CP Umesh, JMJ Paulusse, H Zuilhof, and T Gregorkiewicz. Surface brightens up si quantum dots: direct bandgap-like size-tunable emission. *Light: Science & Applications*, 2:1–6, 2013.

[11] MV Wolkin, J Jorne, PM Fauchet, G Allan, and C Delerue. Electronic states and luminescence in porous silicon quantum dots: the role of oxigen. *Physical review letters*, 82:197–200, 1999.

[12] I Pelant and J Valenta. *Luminescence spectroscopy of semiconductors*. OUP Oxford, 2012.

[13] VI Klimov, AA Mikhailovsky, DW McBranch, CA Leatherdale, and MG Bawendi. Quantization of multiparticle auger rates in semiconductor quantum dots. *Science*, 287(5455):1011–1013, 2000.

[14] C Delerue, M Lannoo, G Allan, E Martin, I Mihalcescu, JC Vial, R Romestain, F Muller, and A Bsiesy. Auger and coulomb charging effects in semiconductor nanocrystallites. *Physical review letters*, 75(11):2228, 1995.

[15] O Guillois, N Herlin-Boime, C Reynaud, Gilles Ledoux, and F Huisken. Photoluminescence decay dynamics of noninteracting silicon nanocrystals. *Journal of applied physics*, 95(7):3677–3682, 2004.

[16] E Rosencher and B Vinter. *Optoelectronics*. Cambridge University Press, 2002.

[17] KL Shaklee and RF Leheny. Direct determination of optical gain in semiconductor crystals. *Applied physics letters*, 18:475–477, 1971.

[18] L Dal Negro, P Bettotti, M Cazzanelli, D Pacifici, and L Pavesi. Applicability conditions and experimental analysis of the variable stripe length method for gain measurements. *Optics communications*, 229(1):337–348, 2004.

[19] NN Ha, K Dohnalová, T Gregorkiewicz, and J Valenta. Optical gain of the 1.54 μm emission in mbe-grown si: Er nanolayers. *Physical Review B*, 81(19):195206, 2010.

[20] J Valenta, I Pelant, and J Linnros. Waveguiding effects in the measurement of optical gain in a layer of si nanocrystals. *Applied physics letters*, 81:1396–1398, 2002.

[21] K Dohnalová. *Study of optical amplification in silicon based nanostructures, Ph.D. Thesis*. PhD thesis, Charles University, Prague & Universit Louis Pasteur, Strasbourg, 2007.

[22] O Svelto, S Taccheo, and C Svelto. Analysis of amplified spontaneous emission: some corrections to the linford formula. *Optics communications*, 149(4):277–282, 1998.

[23] L Ruizendaal, SP Pujari, V Gevaerts, JMJ Paulusse, and H Zuilhof. Biofunctional silicon nanoparticles by means of thiol-ene click chemistry. *Chemistry-an Asian Journal*, 6(10):2776, 2011.

[24] C-S Yang, RA Bley, SM Kauzlarich, HWH Lee, and GR Delgado. Synthesis of alkyl-terminated silicon nanoclusters by a solution route. *Journal of the American Chemical Society*, 121(22):5191–5195, 1999.

[25] D Jurbergs, E Rogojina, L Mangolini, and U Kortshagen. Silicon nanocrystals with ensemble quantum yields exceeding 60 %. *Applied physics letters*, 88:233116, 2006.

[26] AK Gaigalas, L Wang, H-J He, and P DeRose. Procedures for wavelength calibration and spectral response correction of ccd array spectrometers. *Journal of Research of the National Institute of Standards and Technology*, 114(4):215–228, 2009.

[27] CJ Sansonetti, ML Salit, and J Reader. Wavelengths of spectral lines in mercury pencil lamps. *Applied optics*, 35(1):74–77, 1996.

[28] JR Siekierzycka, M Rosso-Vasic, H Zuilhof, and AM Brouwer. Photophysics of n-butyl-capped silicon nanoparticles. *The Journal of Physical Chemistry C*, 115(43):20888–20895, 2011.

[29] K Dohnalová, A Fučíková, CP Umesh, J Humpolíčková, JMJ Paulusse, J Valenta, H Zuilhof, M Hof, and T Gregorkiewicz. Microscopic origin of the fast blue-green luminescence of chemically synthesized non-oxidized silicon quantum dots. *Small*, 8:3185–3191, 2012.